Derivation of the Consistent Osmotic Virial Equation and Its Application to Aqueous Poly(ethylene glycol)–Dextran Two-Phase Systems

Frank Döbert, Andreas Pfennig,* and Matthias Stumpf

Institut für Chemische Technologie, Technische Hochschule Darmstadt, Petersenstrasse 20, D-64287 Darmstadt, Germany

Received June 13, 1994; Revised Manuscript Received June 2, 1995[⊗]

ABSTRACT: Based on the osmotic virial equation by McMillan and Mayer, thermodynamically consistent expressions for the Gibbs free energy of mixing and the chemical potentials of the solutes are derived. In this derivation the concentration dependence of the specific volume is accounted for explicitly. The omostic virial coefficients are determined from water-activity data in binary and ternary solutions of poly(ethylene glycol) and dextran of various molecular weights. This consistent osmotic virial equation is then tested to predict the liquid–liquid equilibria of the ternary systems. On the basis of the parameters obtained solely from water activities the concentrations as well as the molecular-weight distributions of the polymers in the coexisting liquid phases of the aqueous two-phase systems can be predicted in good agreement with the experimental data.

1. Introduction

The osmotic virial equation by McMillan and Mayer[1] has been used successfully to describe the osmotic pressure or equivalently the chemical potential of the solvent in polymer solutions.[2,3] However, the corresponding expressions for the chemical potentials of the solutes are generally derived without considering the concentration dependence of the molar volume of the solution.[4–6]

Based on these expressions for the chemical potentials of the components, the liquid–liquid equilibria in aqueous PEG–dextran two-phase systems were calculated by various authors. This is a system which can be used for the extractive purification of easily denaturing biomolecules such as enzymes.[7,8] The first calculations were performed by Edmond and Ogston.[5] For their calculations they used the binary osmotic virial coefficients A_{22} and A_{33} determined from water-activity data, while the osmotic cross virial coefficient A_{23} was fitted to experimental liquid–liquid equilibrium data. However, the representation of the liquid–liquid equilibria was not satisfactory. E.g. the experimentally determined slopes of the tie lines differ from those calculated and the calculated dextran concentration in the PEG-rich top phase is much too low.

Haynes et al.[9] realized that the third osmotic virial coefficients cannot be neglected for the description of the thermodynamic behavior of aqueous PEG–dextran two-phase systems. But even the introduction of the third osmotic virial coefficients did not lead to a significant increase in the accuracy of the thermodynamic description of this system.

Shishov et al.[10] and especially Kang and Sandler[11] suggested that the deviations between calculation and experiment result from neglecting the polydispersity and the fractionation of the polymers. To account for the polydispersity in the thermodynamic modeling of the aqueous two-phase systems, Kang and Sandler represented the polymers as mixtures of pseudocomponents with various molecular weights using the UNIQUAC model. In fact, considering the polydispersity in the calculations led to a good representation of the liquid–liquid equilibrium data.[11] However, Kang and Sandler demonstrated only the general influence of the polydispersity on the liquid–liquid equilibrium behavior since they used hypothetical molecular-weight distributions of the polymers and neglected the influence of the total composition of the aqueous PEG–dextran system on the liquid–liquid equilibria.

The goal of this work is to construct a thermodynamic function from the osmotic virial equation by McMillan and Mayer which is capable of simultaneously describing vapor–liquid as well as liquid–liquid equilibrium data. The severest test of this thermodynamic model is the prediction of the liquid–liquid equilibria with model parameters determined solely from experimental information on the vapor–liquid equilibrium, since such a prediction generally fails for mixtures of components of low molecular weight.

Thus, in a first step, thermodynamically consistent expressions for the chemical potentials of the solutes and the Gibbs free energy of mixing are derived from the McMillan–Mayer equation. Special care is taken to account for the concentration dependence of the molar volume of the solution. In a next step the osmotic virial coefficients for the system water + PEG + dextran are determined from water-activity data over the entire mixing range of these systems reported previously.[12] On the basis these osmotic virial coefficients the liquid–liquid equilibrium behavior of the aqueous PEG–dextran two-phase systems including the compositions and the molecular-weight distributions of the polymers in the coexisting phases can be predicted and compared to experimental data.[13] This comparison allows us to judge the quality of the derived model and the importance of various factors such as, e.g., the polydispersity of the polymers.

2. Theory

2.1. Derivation of Thermodynamically Consistent Expressions for the Chemical Potentials of the Solutes Based on the McMillan–Mayer Equation. The osmotic virial equation has been developed by McMillan and Mayer for solutions of nonelectrolytes.[1] In this model the osmotic pressure π is expressed as a

[⊗] Abstract published in *Advance ACS Abstracts,* September 15, 1995.

0024-9297/95/2228-7860$09.00/0

power series in the concentration c_i of the solutes in moles of i per cubic centimeter of solution:

$$\frac{\pi}{RT} = \sum_{i=2}^{N} c_i + \sum_{i=2}^{N}\sum_{j=2}^{N} A_{ij} c_i c_j + \sum_{i=2}^{N}\sum_{j=2}^{N}\sum_{k=2}^{N} A_{ijk} c_i c_j c_k + \ldots \quad (1)$$

where index 1 represents the solvent, while the indices 2 to N refer to the solutes. Here the A_{ij} und A_{ijk} are the second and third osmotic virial coefficients which have to be determined from experimental data. The osmotic virial coefficients express the interactions between two or three molecules of the solutes i, j, and k surrounded by the solvent. The osmotic virial coefficients depend on polymer molecular weight and temperature.

Using the relation $-\pi\bar{V}_1^0 = \mu_1 - \mu_1^0(T,P)$,[14] the corresponding expression for the chemical potential of the solvent μ_1 at constant P and T is

$$\frac{\mu_1 - \mu_1^0(T,P)}{RT\bar{V}_1^0} = -\sum_{i=2}^{N}\frac{\rho_i}{M_i} - \sum_{i=2}^{N}\sum_{j=2}^{N}\frac{A_{ij}\rho_i\rho_j}{M_i M_j} - \sum_{i=2}^{N}\sum_{j=2}^{N}\sum_{k=2}^{N}\frac{A_{ijk}\rho_i\rho_j\rho_k}{M_i M_j M_k} - \ldots \quad (2)$$

where $\mu_1^0(T,P)$ is the chemical potential of the pure solvent at P and T, $\bar{V}_1^0$ is the molar volume of the pure solvent, R is the gas constant, and T is the temperature. In (2) the concentration c_i has been replaced by the mass concentrations ρ_i in grams of i per milliliter of solution, since the concentrations of the polymer solutes c_i are very small because of the high molecular weight of the polymers:

$$\rho_i = c_i M_i = \frac{x_i M_i}{V} \quad (3)$$

Here the molar volume of the solution

$$V = \sum_{i=1}^{N} x_i \bar{V}_i^0 \quad (4)$$

is described in the investigated concentration range by excluding excess volumes, as verified in Appendix 1.

With this assumption the molar Gibbs free energy of mixing G^M can be derived from (2) by integration:

$$G^M = \frac{1}{n}\left(\int(\mu_1 - \mu_1^0)\, dn_1 + C(T,P,n_2,n_3,\ldots,n_N)\right) \quad (5)$$

Here $C(T,P,n_2,n_3,\ldots,n_N)$ is an integration constant wich can be determined using the Gibbs–Duhem equation for an isobaric–isothermal system,

$$\sum_{i=1}^{N} n_i \left(\frac{\partial \mu_i}{\partial n_j}\right)_{T,P,n_{i\neq j}} = 0 \quad \text{for} \quad j = 1, 2, \ldots, N \quad (6)$$

with

$$\mu_i - \mu_i^0 = \left(\frac{\partial n G^M}{\partial n_i}\right)_{T,P,n_{j\neq i}} \quad (7)$$

and the condition that the Gibbs free energy of mixing G^M of the pure components is zero,

$$G^M(x_i = 1) = 0 \quad \text{for} \quad i = 1, 2, \ldots, N \quad (8)$$

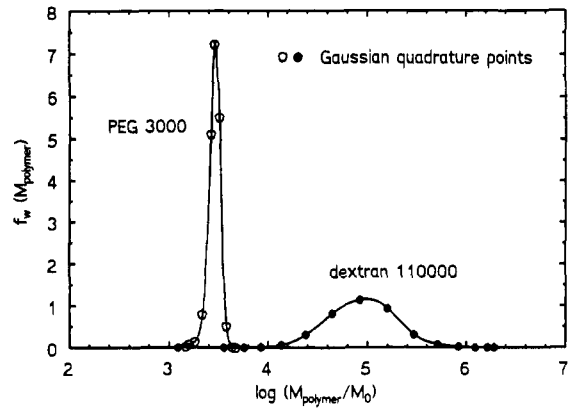

Figure 1. Molecular-weight distribution of PEG 3000 and dextran 110 000.

From (2)–(8) the following consistent osmotic virial equation (COVE) for G^M is obtained:

$$\frac{G^M}{RT} = \sum_{i=2}^{N} x_i \ln\frac{x_i\bar{V}_i^0}{V} + \sum_{i=2}^{N}\sum_{j=2}^{N} A_{ij}\frac{x_i x_j}{V} + \frac{1}{2}\sum_{i=2}^{N}\sum_{j=2}^{N}\sum_{k=2}^{N} A_{ijk}\frac{x_i x_j x_k}{V^2} - \sum_{i=2}^{N} A_{ii}\frac{x_i}{\bar{V}_i^0} - \frac{1}{2}\sum_{i=2}^{N} A_{iii}\frac{x_i}{(\bar{V}_i^0)^2} \quad (9)$$

For the chemical potentials of the solutes μ_z follows with (7):

$$\frac{\mu_z - \mu_z^0(T,P)}{RT} = \ln\frac{\rho_z\bar{V}_z^0}{M_z} + \sum_{i=2}^{N}\left(2\frac{A_{iz}}{M_i} - \frac{\bar{V}_z^0}{M_i}\right)\rho_i + \sum_{i=2}^{N}\sum_{j=2}^{N}\left(\frac{3A_{ijz}}{2M_i M_j} - \frac{\bar{V}_z^0 A_{ij}}{M_i M_j}\right)\rho_i\rho_j - \sum_{i=2}^{N}\sum_{j=2}^{N}\sum_{k=2}^{N}\frac{\bar{V}_z^0 A_{ijk}}{M_i M_j M_k}\rho_i\rho_j\rho_k \quad (10)$$

where $\mu_z^0(T,P)$ refers to the chemical potential of the pure solute z in a hypothetical liquid state.

2.2. Polydispersity. The fact that synthetic polymers are polydisperse components has considerable influence on the phase behavior of the polymer solutions.[15] The molecular-weight distribution of the polymers used in our work is illustrated in Figure 1 for PEG 3000 and dextran 110 000, where the numbers refer to the weight-average molecular weight of the polymers. The molecular-weight distributions $f_w = dw_i/d\log(M_i/M_0)$ with $M_0 = 1$ g/mol have been determined using size-exclusion chromatography (SEC).[13] Figure 1 shows that dextran has a wide molecular-weight distribution, while the polydispersity of PEG is negligible.

In the modeling, the molecular-weight distribution can be accounted for by applying the concepts of continuous thermodynamics, as introduced by Kehlen and Rätzsch[16] as well as Cotterman et al.[17,18] Following these authors, the experimentally determined distribution can be represented by a small number of pseudocomponents, which are also shown in Figure 1. The 15 pseudocomponents were systematically chosen using the Gaussian quadrature method.[19]

3. Determination of the Osmotic Virial Coefficients from Water-Activity Data

The osmotic virial coefficients were determined from water-activity data of the aqueous PEG–dextran sys-

Table 1. Model Parameters for the System Water (1) + PEG (2) with $c_{ii} = 0.819$

T (K)	$10^3 a_{ii}$ [(cm^3 mol)/g^2]	b_{ii} [(cm^6 mol)/g^3]	$10^2 a_{iii}$ [(cm^3 mol)/g^2]	$10 b_{iii}$ [(cm^6 mol)/g^3]	c_{iii}
293.15	2.174	0.374	0.409	0.326	0.134
313.15	1.502	0.253	0.299	0.453	0.195
333.15	1.031	0.246	0.245	0.746	0.283

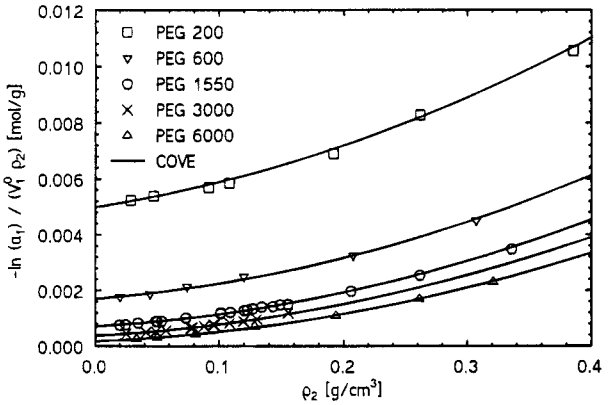

Figure 2. Reduced excess chemical potential of water as a function of ρ_2 for the system water (1) + PEG (2) at 293.15 K.

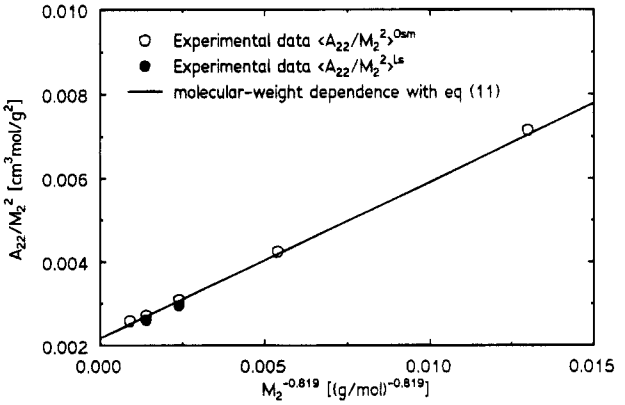

Figure 3. Second osmotic virial coefficients of the system water (1) + PEG (2) at 293.15 K.

tems. These data have been measured over the entire homogeneous mixing range of the system, as reported previously.[12] The measurements were performed with two vapor-pressure osmometers (Knauer, Berlin and GONOTEC, Berlin) and a membrane osmometer for dextran solutions (GONOTEC, Berlin). In a first step, the binary osmotic virial coefficients A_{ii} and A_{iii} were fitted to the water-activity data of the systems water + PEG and water + dextran. The osmotic virial coefficients for both binary systems decrease with increasing polymer molecular weight.[3,12]

To describe this molecular-weight dependence, it has been assumed that the second and third osmotic virial coefficients can be expressed as[20,21]

$$\frac{A_{ii}}{M_i^2} = a_{ii} + b_{ii} M_i^{-c_{ii}} \tag{11}$$

$$\frac{A_{iii}}{M_i^3} = a_{iii} + b_{iii} M_i^{-c_{iii}} \tag{12}$$

a_{ii}, b_{ii}, and c_{ii} as well as a_{iii}, b_{iii}, and c_{iii} being the model parameters. Experimental investigations of solutions of monodisperse polymers have shown that the molecular-weight dependence can be well described using (11) and (12).[2,20,22-26]

Since the PEGs investigated are essentially monodisperse, all model parameters in (11) and (12) for PEG were fitted to the water-activity data of PEG solutions by a least-squares method. It turned out that the temperature dependence of the model parameter c_{ii} can be neglected without any loss in accuracy. This parameter was adjusted separately, resulting in the value $c_{ii} = 0.819$. The remaining parameters are given in Table 1. Obviously, the exponent c_{iii} is much smaller than c_{ii}. This indicates that the molecular-weight dependence of the third osmotic virial coefficient is less pronounced than that of the second osmotic virial coefficient.

The water-activity data of aqueous PEG-solutions can be represented well using (11) and (12), as shown in Figure 2. Figure 3 demonstrates the good agreement between the second osmotic virial coefficients calculated with (11) and (12) and those determined experimentally by osmometry[12] and light scattering. The light-scattering measurements have been performed in collaboration with Professor G. Wegner at the Max-Planck-Institut für Polymerforschung, Mainz, and are evaluated in detail in Appendix 2.

For the polydisperse dextran the osmotic virial coefficients determined by various experimental techniques represent different averages over the distribution of chain lengths. With osmotic measurements the following average of the second osmotic virial coefficient is obtained:[21,22]

$$\left\langle \frac{A_{ii}}{M_i^2} \right\rangle^{\mathrm{Osm}} = \frac{1}{M_{n,i}^2} \int_0^\infty \int_0^\infty A_{i_\alpha i_\beta} f_n(M_{i_\alpha}) f_n(M_{i_\beta}) \, \mathrm{d}\log\frac{M_{i_\alpha}}{M_0} \, \mathrm{d}\log\frac{M_{i_\beta}}{M_0} \tag{13}$$

where $f_n(M_i)$ is defined as $\mathrm{d}x_i/\mathrm{d}\log(M_i/M_0)$ and $A_{i_\alpha i_\beta}$ describes the interaction between the polymer chains of the same chemical species with different molecular weights distinguished by the indices α and β. On the other hand, from light-scattering measurements the following average of the second osmotic virial coefficient can be deduced:[21,22]

$$\left\langle \frac{A_{ii}}{M_i^2} \right\rangle^{\mathrm{Ls}} = \frac{1}{M_{\mathrm{w},i}^2} \int_0^\infty \int_0^\infty A_{i_\alpha i_\beta} f_{\mathrm{w}}(M_{i_\alpha}) f_{\mathrm{w}}(M_{i_\beta}) \, \mathrm{d}\log\frac{M_{i_\alpha}}{M_0} \, \mathrm{d}\log\frac{M_{i_\beta}}{M_0} \tag{14}$$

In Figure 4, these average second osmotic virial coefficients of aqueous dextran solutions from osmotic and light-scattering measurements, $\langle A_{33}/M_3^2\rangle^{\mathrm{Osm}}$ [12] and $\langle A_{33}/M_3^2\rangle^{\mathrm{Ls}}$ (see Appendix 2), are compared.

When the osmotic virial equation is applied to solutions of the polydisperse dextran, the interactions between two polymer molecules of different chain

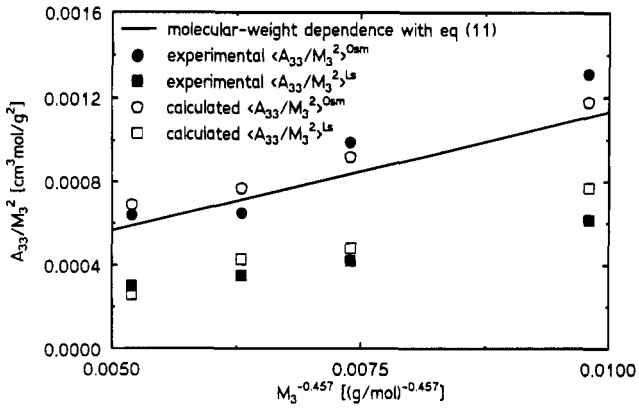

Figure 4. Second osmotic virial coefficients of the system water (1) + dextran (3) at 293.15 K as a function of the dextran molecular weight.

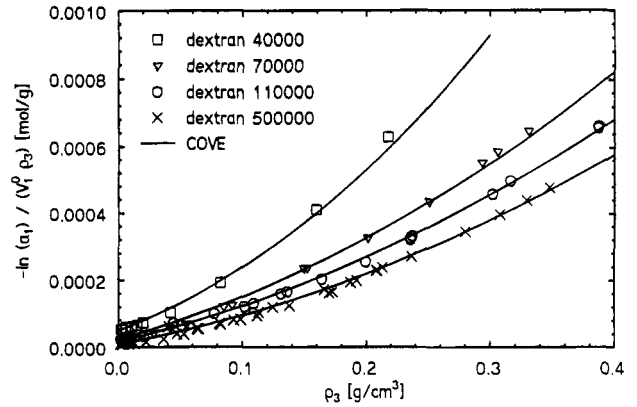

Figure 5. Reduced excess chemical potential of water as a function of ρ_3 for the system water (1) + dextran (3) at 293.15 K.

Table 2. Model Parameters for the System Water (1) + Dextran (3) with $a_{ii} = b_{iii} = c_{iii} = 0$

T (K)	b_{ii} [(cm^6 mol)/g^3]	c_{ii}	$10^2 a_{iii}$ [(cm^3 mol)/g^2]
293.15	0.113	0.457	0.274
313.15	0.190	0.465	0.231
333.15	0.186	0.636	0.240

lengths have to be considered explicitly. To determine the corresponding cross coefficients, Casassa[27] introduced an empirical correlation based on a hard-sphere model. However, the correlations of Casassa did not result in a good description of the thermodynamic behavior of the aqueous dextran solutions.

When the interactions between two dextran molecules α and β are described using the following relations, the thermodynamic behavior of the dextran solutions can be described well:

$$A_{i_\alpha i_\beta} = (A_{i_\alpha i_\alpha} A_{i_\beta i_\beta})^{1/2} \tag{15}$$

$$A_{i_\alpha i_\beta i_\gamma} = (A_{i_\alpha i_\alpha i_\alpha} A_{i_\beta i_\beta i_\beta} A_{i_\gamma i_\gamma i_\gamma})^{1/3} \tag{16}$$

where $A_{i_\alpha i_\alpha}$ and $A_{i_\alpha i_\alpha i_\alpha}$ are calculated for dextran of the molecular weight M_{i_α} from (11) and (12).

On the basis of (11), (12), (15), (16), and the experimental molecular-weight distributions of the dextran, all parameters of the model were simultaneously fitted to the water-activity data. As a result, the molecular-weight dependence of the third osmotic virial coefficient turned out to be negligible and thus b_{iii} and c_{iii} were set equal to zero. Also the coefficient a_{ii} is zero. The remaining coefficients of (11) and (12) for dextran are given in Table 2.

Using these parameters, a good description of the experimentally determined water-activity data is obtained, as shown in Figure 5. As can be seen in Figure 4, the calculated average virial coefficients, both $\langle A_{33}/M_3^2\rangle^{Osm}$ and $\langle A_{33}/M_3^2\rangle^{Ls}$, are also in good agreement with the experimental results. The quality of the model is demonstrated in particular by the good agreement between the experimental and the calculated average light-scattering osmotic virial coefficients, since the calculated values represent a true prediction.

In a next step this model was extended to the ternary system water + PEG + dextran. Here again it was assumed that the molecular-weight dependence of the osmotic cross virial coefficients can be described with (11) and (12). Because of the specific interactions between the two different types of solutes i and j, we additionally introduced the coefficients $\xi_{i_\alpha j_\beta}$ and $\xi_{i_\alpha j_\beta k_\gamma}$ in order to generalize (15) and (16). The resulting equations for the osmotic cross virial coefficients are

$$A_{i_\alpha j_\beta} = \xi_{i_\alpha j_\beta} (A_{i_\alpha i_\alpha} A_{i_\beta i_\beta})^{1/2} \tag{17}$$

$$A_{i_\alpha j_\beta k_\gamma} = \xi_{i_\alpha j_\beta k_\gamma} (A_{i_\alpha i_\alpha i_\alpha} A_{j_\beta j_\beta j_\beta} A_{k_\gamma k_\gamma k_\gamma})^{1/3} \tag{18}$$

where the coefficients $\xi_{i_\alpha j_\beta}$ and $\xi_{i_\alpha j_\beta k_\gamma}$ depend on the molecular weight of the polymers as expressed by

$$\xi_{i_\alpha i_\beta} = 1 \tag{19}$$

$$\xi_{i_\alpha i_\beta i_\gamma} = 1 \tag{20}$$

$$\xi_{2_\alpha 3_\beta} = \xi^{(1)}_{23} + \xi^{(2)}_{23} M_{2_\alpha} + \xi^{(3)}_{23} M_{3_\beta} \tag{21}$$

$$\xi_{2_\alpha 2_\beta 3_\gamma} = \xi^{(1)}_{223} + \xi^{(2)}_{223} (M_{2_\alpha} M_{2_\beta})^{1/2} + \xi^{(3)}_{223} M_{3_\gamma} \tag{22}$$

$$\xi_{2_\alpha 3_\beta 3_\gamma} = \xi^{(1)}_{233} + \xi^{(2)}_{233} M_{2_\alpha} + \xi^{(3)}_{233} (M_{3_\beta} M_{3_\gamma})^{1/2} \tag{23}$$

These relations can easily be extended to systems containing an arbitrary number of components.

The coefficients $\xi^{(l)}_{ij}$ and $\xi^{(l)}_{ijk}$ obtained from a least-squares fit to the experimental water-activity data of the ternary mixtures are presented in Table 3. The good agreement between calculated and measured water activities for the system water + PEG 3000 + dextran 110 000 is shown in Figure 6. Additionally, the calculated water activities from a fit to the data for this system, where the molecular-weight dependence of the

Table 3. Correction Factors $\xi^{(l)}_{ij}$ and $\xi^{(l)}_{ijk}$ of (20)–(24) in the Ternary System Water (1) + PEG (2) + Dextran (3)[a]

T (K)	$\xi^{(1)}_{223}$	$10^4\xi^{(2)}_{223}$ (mol/g)	$10^6\xi^{(3)}_{223}$ (mol/g)	$\xi^{(1)}_{233}$	$10^4\xi^{(2)}_{233}$ (mol/g)	$10^6\xi^{(3)}_{233}$ (mol/g)
293.15	0.034	2.704	5.746	0.321	2.195	5.190
313.15	0.241	2.316	4.955	0.375	2.120	9.880
333.15	0.255	0.465	2.336	0.201	0.998	3.014

[a] The correction factors for the second osmotic cross virial coefficient were found to be temperature independent: $\xi^{(1)}_{23} = 2.396$, $\xi^{(2)}_{23} = -2.117 \times 10^{-4}$ (mol/g), and $\xi^{(3)}_{23} = -4.01 \times 10^{-6}$ (mol/g).

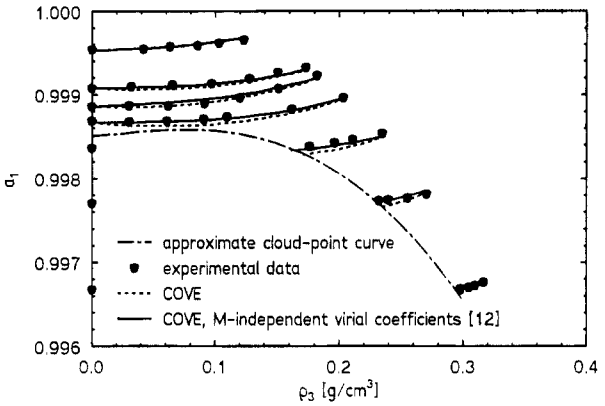

Figure 6. Water activity a_1 as a function of ρ_3 for the system water (1) + PEG 3000 (2) + dextran 110 000 (3) at 293.15 K along seven mixing lines.[12]

Table 4. Enthalpic and Entropic Contributions to the Free Energy of Mixing in Aqueous Polymer Solutions with $w_{polymer} = 0.2$ at 303.15 K

polymer	G^M/RT	H^M/RT	S^M/R
PEG 3000	−0.057	−0.188	−0.131
dextran 110 000	−0.020	−0.048	−0.028

osmotic virial coefficients has been neglected, are included in this plot[12] to show the small differences between this best fit and the fit with the derived model.

Thus, a function has been constructed, which allows us to describe the chemical potentials of water as well as those of the polymers in aqueous PEG–dextran solutions as a function of molecular weight and the molecular-weight distribution of the polymers.

4. Calculation of the Enthalpy and Entropy of Mixing

The temperature dependence of the parameters can now be used to determine the enthalpy and entropy of mixing of aqueous PEG–dextran solutions by numerical differentiation of (9). The values of H^M, TS^M, and G^M calculated from the COVE model with the parameters presented are shown in Table 4. The negative values of TS^M indicate that the mixing of water with the polymers in a hypothetically liquid state leads to a strong ordering of the solution, especially in the case of PEG. This negative TS^M is compensated by an even more negative H^M to result in negative values of G^M. The negative H^M results from strong energetic interactions which are formed in the mixture. Thus it appears that, upon mixing, the structure of the solution is increased in a way which maximizes the number of hydrogen bonds. This effect is especially pronounced in PEG solutions and is in accordance with results of Florin and Kjellander.[28] They suggested a strong structuring of PEG dissolved in water, where hydrogen bonds between the ether oxygens of the PEG and the surrounding water molecules are formed while the ethylene groups of the PEG form cages which are free of water. This structure can be achieved by a helical conformation of PEG in aqueous solution.[28]

5. Prediction of the Liquid–Liquid Equilibrium Behavior

With COVE and the parameters given, it is possible to predict the liquid–liquid equilibrium in aqueous PEG–dextran two-phase systems. The calculations of

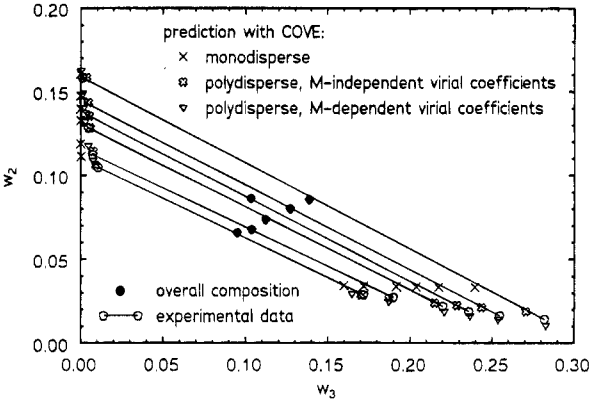

Figure 7. Predicted and experimental phase diagram of the system water (1) + PEG 3000 (2) + dextran 110 000 (3) at 293.15 K.

the liquid–liquid equilibria were performed using a modified flash algorithm developed by Topliss.[29] In this algorithm, the phase compositions and the molecular-weight distributions of the polymers in the coexisting phases are calculated for a given overall composition and temperature of the system.[30] The routines by Topliss use a combination of a first- and second-order algorithm to efficiently solve the equilibrium conditions and the material balances.

5.1. Results of the Predictions. The predictions using COVE are discussed here for the system water + PEG 3000 + dextran 110 000. To show the dramatic influence of the polydispersity and the fractionation of the polymers on the prediction of the liquid–liquid equilibria, the phase behavior has also been predicted with both polymers treated as monodisperse components. For this prediction, the osmotic virial coefficients have been determined from water-activity data by assuming monodispersity of PEG and dextran, as reported previously.[12,31] The predicted compositions in the PEG-rich top phase and the dextran-rich bottom phase are shown in Figure 7 in a concentration diagram and compared to the experimentally determined phase compositions. This comparison shows that the predicted concentration of dextran in the PEG-rich top phase is much too low with a monodisperse calculation. The reason for this is that the effect of fractionation of the polydisperse dextran in this monodisperse treatment is neglected. Thus the molecular weight of dextran in the PEG-rich top phase is overestimated and for the same reason the compatibility and the concentration of dextran in this phase are underestimated.[13]

In the next step the polydispersity of dextran was considered in predictions of the liquid–liquid equilibria in the aqueous PEG–dextran solutions, but the osmotic virial coefficients A_{ij}/M_iM_j and $A_{ijk}/M_iM_jM_k$ were still kept molecular-weight independent. For a direct comparison with the monodisperse prediction, these calculations were carried out with the same osmotic virial coefficients as in the monodisperse treatment. The prediction of the phase compositions based on these assumptions is in good agreement with the experimental results in the top as well as in the bottom phase, as can be seen in Figure 7.

The shortcomings of these model assumptions turn up when the predicted molecular-weight distributions of dextran in the coexisting phases are considered, as shown in Figure 8. The molecular-weight distributions

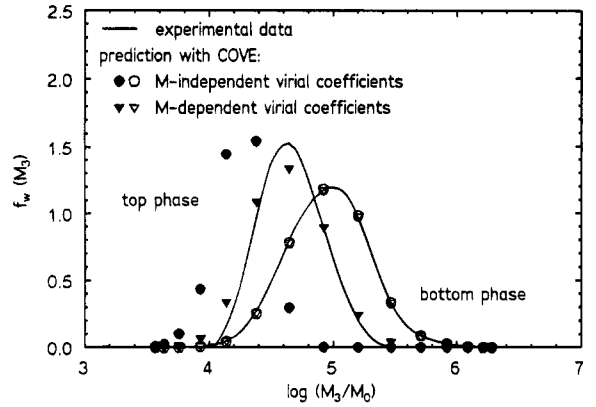

Figure 8. Predicted and experimental molecular-weight distributions of dextran for a tie line of intermediate length in the system water (1) + PEG 3000 (2) + dextran 110 000 (3) at 293.15 K.

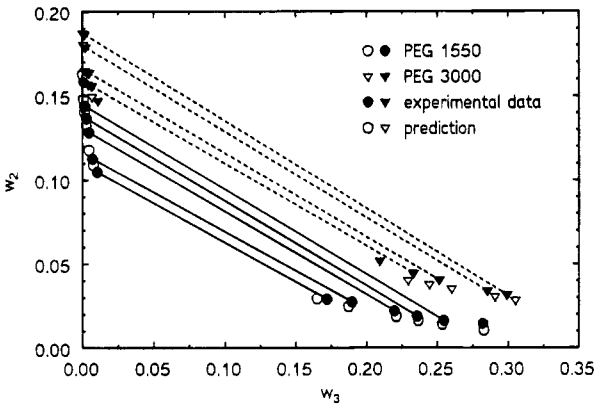

Figure 9. Predicted and experimental phase diagrams of the system water (1) + PEG (2) + dextran 110 000 (3) at 293.15 K as a function of molecular weight of PEG.

of dextran in the dextran-rich bottom phase for both experiment and prediction are essentially equal to that of the pure dextran, since almost all of the dextran partitions into the dextran-rich bottom phase. In the PEG-rich top phase the dextran concentration is very low and preferentially dextrans of low molecular weight are found in this phase. However, the fractionation of dextran is overestimated in these predictions if the molecular-weight dependence of the osmotic virial coefficients is neglected.

Finally, COVE was applied without any simplifications as presented in the previous sections to describe the thermodynamic behavior in the system water + PEG 3000 + dextran 110 000, as also shown in Figures 7 and 8. With COVE the phase compositions as well as the molecular-weight distributions of dextran in the coexisting phases can be predicted in good agreement with the experimental results. This indicates that primarily the fractionation effect is influenced by the introduction of the explicit and correct molecular-weight dependence of the osmotic virial coefficients.

The derived model can now be used to predict the liquid–liquid equilibrium behavior of aqueous PEG–dextran systems with varying molecular weights of the polymers, as shown in Figures 9 and 10. The good agreement indicates the high quality of the COVE model.

5.2. Influence of the Phase Ratio on the Liquid–Liquid Equilibrium Behavior. So far all predictions of the liquid–liquid equilibrium behavior were per-

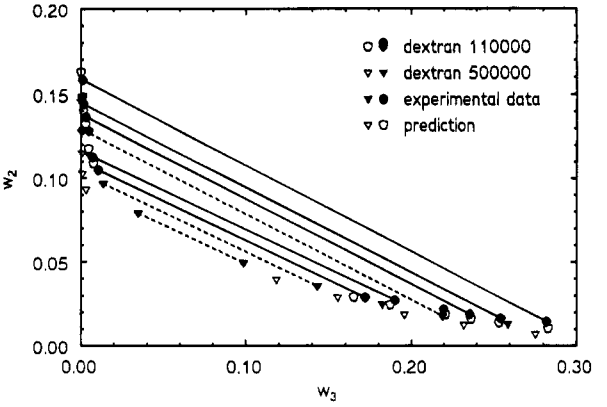

Figure 10. Predicted and experimental phase diagrams of the system water (1) + PEG 3000 (2) + dextran (3) at 293.15 K as a function of molecular weight of dextran.

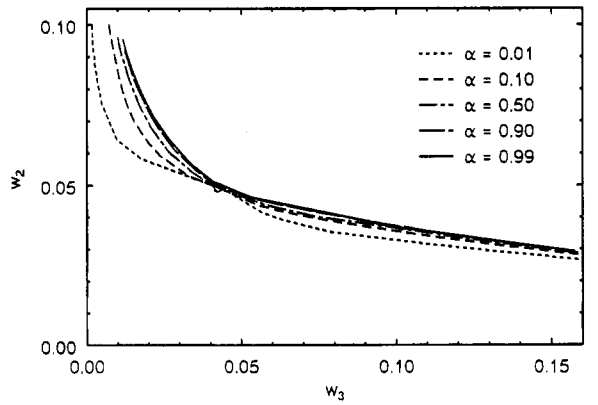

Figure 11. Predicted coexistence curve of the system water (1) + PEG 3000 (2) + dextran 110 000 (3) at 293.15 K as a function of the phase ratio α.

formed for the same overall compositions of the aqueous two-phase systems as in the experimental investigations by Connemann et al.[13] These overall compositions were chosen such that the volume ratio of the phases formed is close to unity. However, the phase ratio has a strong influence on the liquid–liquid equilibria.[12] In the experiment the coexistence curve for a phase ratio of approximately 0.5, where α is defined as

$$\alpha = \frac{\text{mass of the bottom phase}}{\text{total mass of the system}} \qquad (24)$$

differs dramatically from the cloud-point curve of the system.[12] This difference can be explained by polydispersity effects.[15]

To gain more insight into the physicochemical basis of this behavior, the coexistence curves of the system water + PEG 3000 + dextran 110 000 were calculated for various phase ratios α. The resulting coexistence curves are illustrated in Figure 11 in a concentration diagram. Corresponding to this phase diagram, in Figure 12 the calculated weight-average molecular weights M_w of dextran are shown as a function of the tie-line length, which is defined as $(\Delta w_2^2 + \Delta w_3^2 - \Delta w_2 \Delta w_3)^{1/2}$, where Δw_i is the difference of the weight fractions of component i between the coexisting phases.

Figures 11 and 12 show that the coexistence curve is strongly influenced by α and that this influence corresponds to a shift of the fractionation of dextran between the coexisting phases. This can be seen in particular

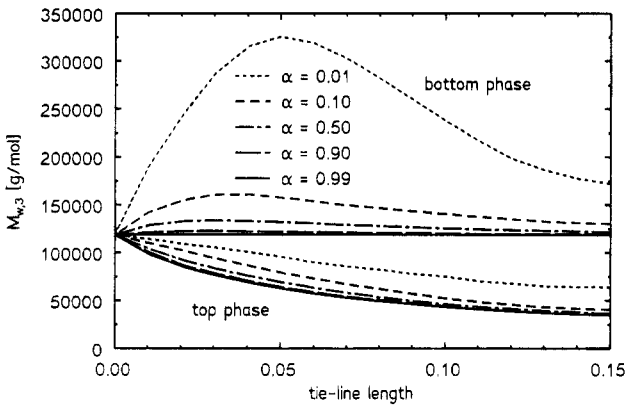

Figure 12. M_w of dextran in the coexisting phases as a function of the tie-line length and the phase ratio α of the system water (1) + PEG 3000 (2) + dextran 110 000 (3) at 293.15 K.

for a phase ratio α = 0.01, where M_w is shifted to very high values especially in the bottom phase. This high average molecular weight results in a low compatibility with PEG in water and a coexistence curve which is very large for this phase ratio. Conversely, for a phase ratio of 0.99, M_w of dextran in both phases is shifted toward lower values and correspondingly the coexistence curve is shifted to higher polymer concentrations. Thus, on the basis of these calculations for various phase ratios α, the differences between the experimentally determined cloud-point curve and the coexistence curves can be understood.

It can also be seen in Figure 12 that the molecular-weight distribution of dextran in the coexisting phases depends strongly on the tie-line length. For long tie lines the M_w of dextran in the bottom phase equals almost that of the pure component distribution, while M_w in the top phase is very small. This fractionation effect is due to the incompatibility of the dextrans of high molecular weight with PEG in aqueous solution and the low dextran concentration in the PEG-rich top phase, as pointed out in section 5.1. For shorter tie lines the dextran concentration in the PEG-rich top phase increases. This can only be achieved by the partitioning of dextran of higher molecular weight into the top phase. Thus, the average molecular weight of dextran in the top phase increases as the tie lines become shorter. Also the average molecular weight of dextran M_w in the bottom phase increases, since more dextran of low molecular weight as compared to the pure dextran distribution partitions into the top phase. For very short tie lines even dextran fractions with very high molecular weights are compatible with the PEG-rich top phase, because the phase compositions as well as the molecular-weight distributions of the coexisting phases approach each other at the critical demixing point.

Acknowledgment. The authors are grateful to Professor Dr. G. Wegner and Dr. M. Schmidt at the Max-Planck-Institut für Polymerforschung, Mainz, for their assistance in performing and evaluating the light-scattering experiments. Further, we thank the Deutsche Forschungsgemeinschaft for financial support.

6. Symbols

a_1	activity of solvent, here water
A_{ij}	second osmotic virial coefficient
A_{ijk}	third osmotic virial coefficient
c_i	amount of substance concentration of component i
G^M	molar Gibbs free energy of mixing
M	molecular weight
N	number of components
n	number of moles of total system
n_i	number of moles of component i
R	gas constant
T	temperature
$\bar{V}_i$	partial molar volume of component i
V	molar volume of the solution
x_i	mole fraction of component i
w_i	weight fraction of component i
α	phase ratio
μ_i	chemical potential of component i
ρ_i	mass concentration of component i

Indices

i	component index
n	number average
w	weight average
0	reference state
1	water
2	PEG
3	dextran

Appendix 1. Concentration Dependence of the Molar Volume of Aqueous PEG–Dextran Solution

Molar volumes of the binary aqueous PEG and dextran solutions have been measured using a density-sound analyzer (type DSA 48, Heräus Paar, Graz) as presented in a previous paper.[12] It turns out that the molar volume is a linear function of the mole fraction in the concentration range investigated. Thus the molar volume of solutions of PEG and dextran V can be calculated as

$$V = \sum_{i=1}^{N} x_i \bar{V}_i^0 \tag{25}$$

where $\bar{V}_i^0$ is the partial molar volume of component i which is constant in this concentration range. Here the index 0 indicates that the value refers to pure water and the polymers at infinite dilution, respectively. The values of $\bar{V}_i^0$ are given in Table 5.[12]

The validity of (25) in the ternary mixing range has been examined in this work. Stock solutions of PEG and dextran were mixed in different ratios, resulting in mixing points which lie on a mixing line in a concentration diagram. The concentrations of the stock solutions were chosen in such a way that these mixing lines are approximately parallel to the experimentally determined tie lines. In Figure 13 the results are shown for two mixing lines. The excess volume of the mixture can be neglected, since the data points corresponding to a mixing line fall on a straight line. Thus (25) can be applied to ternary aqueous solutions of PEG and dextran with good accuracy.

Appendix 2. Static Light Scattering in Binary Aqueous PEG and Dextran Solutions

Static light-scattering measurements have been performed in collaboration with Professor Dr. G. Wegner, Max-Planck-Institut für Polymerforschung, Mainz. The light-scattering apparatus consists of a Kr-ion laser (Λ = 647.1 nm, Spectra Physics, Model 2025) and a

Table 5. Hypothetical Specific Volumes v_i^0 of PEG (2) and Dextran (3)[a]

T (K)	v_2^0 (mL/g)	v_3^0 (mL/g)
293.15	0.8302	0.5959
313.15	0.8573	0.6203
333.15	0.8711	0.6322

[a] The partial molar volumes in the investigated concentration range can be obtained from the relation $\bar{V}_i^0 = v_i^0 M_i$ with the $M_{n,i}$ of the monodisperse PEG given in Table 6 and the M_i of the dextran fractions from the molecular-weight distributions of this polymer.[13]

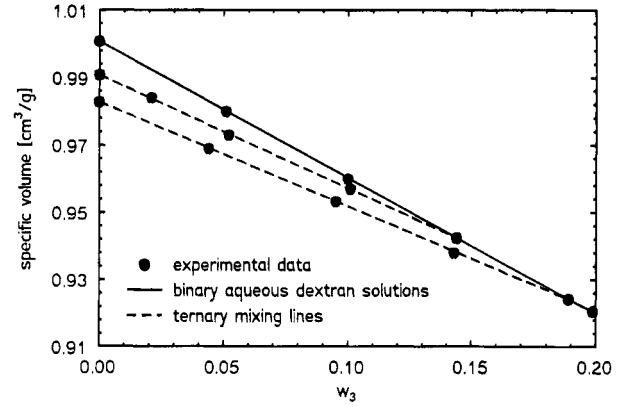

Figure 13. Specific volumes of the solution as a function of the weight fraction of dextran for various mixing lines in the system water (1) + PEG 3000 (2) + dextran 110 000 at 293.15 K.

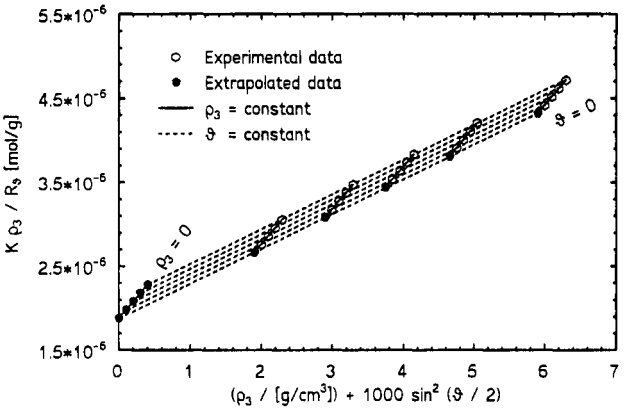

Figure 14. Zimm diagram for the system water + dextran 500 000 at 293.15 K.

goniometer (ALV-SP 52, Spectra Physics). A Sirius-1 microcomputer enables on-line control and evaluation of the measured light-scattering intensities i_ϑ. The scattered light can be measured over the angular range between 26° and 143°.[32]

For the examination of the binary aqueous PEG and dextran solutions, five to six samples varying in concentration were prepared, repeatedly filtered several times through disposable Millipore filters (0.2, 0.45, or 1.2 μm porosity, depending on the molecular weight of the polymer), and then poured into a dust-free cuvette. The solvent was handled in the same way.

According to Zimm, the measured static light-scattering intensities i_ϑ are related to the polymer concentration c_i and the scattering angle ϑ as follows:[33,34]

$$\frac{Kc_i}{R_\vartheta} = \frac{1}{M_{w,i}P_{z,\vartheta}} + 2\left\langle\frac{A_{ii}}{M_i^2}\right\rangle^{Ls} c_i + \ldots \quad \text{for} \quad \frac{\lambda}{20} \le d \le \frac{\lambda}{2} \tag{26}$$

where R_ϑ is the ratio of the scattering intensity i_ϑ at the distance r from the scattering center of the incident light with the intensity I_0:

$$R_\vartheta = \frac{i_\vartheta r^2}{I_0} \tag{27}$$

K is an optical constant, $\langle A_{ii}/M_i^2\rangle^{Ls}$ is the weight-average second osmotic virial coefficient according to eq 14, $M_{w,i}$ is the weight-average molecular weight of the polymer, and $P_{z,\vartheta}$ is the z-average shape factor of the polymer. According to Zimm, the initial angular dependence of $P_{z,\vartheta}$ is given by[33]

$$P_{z,\vartheta} = 1 - \frac{16}{3}\pi^2 n^2 \frac{\langle s_i^2\rangle_z}{\lambda^2}\sin^2\left(\frac{\vartheta}{2}\right) \tag{28}$$

$P_{z,\vartheta}$ is influenced by intramolecular interferences. The experimental values of $P_{z,\vartheta}$ are correlated with the shape and the z-average mean-square radius of gyration $\langle s^2\rangle_z$ of the polymer coil.[33]

As an example, the Zimm diagram is shown for the system water + dextran 500 000 at 293.15 K in Figure 14. The radius of gyration $\langle s^2\rangle_z$, the second osmotic virial coefficient $\langle A_{ii}/M_i^2\rangle^{Ls}$, and the molecular weight of a polymer M_w obtained from this diagram by linear extrapolation are given in Table 6. The radii of gyration $\langle s_i^2\rangle_z^{0.5}$ could not be determined for the PEG in aqueous solution since the molecular weights are far to small for R_ϑ to show an angular dependence.

According to Table 6, the radius of gyration $\langle s_i^2\rangle_z^{0.5}$ of dextran increases with molecular weight. Using the relation

$$\langle s_i^2\rangle_z^{0.5} = C\left(\frac{M_i}{M_0}\right)^a \tag{29}$$

different exponents a are obtained for the different shapes of the polymers. For an unperturbed polymer coil in solution at the Θ-temperature a is 0.5. For dextran in water at temperatures other than the Θ-temperature of 375 K, the dimensions of the polymer will be altered. Then the exponent a will be shifted to slightly higher values with increasing second osmotic virial coefficient.[35] This is in agreement with the value $a = 0.52$ with a constant $C = 2.11 \times 10^{-3}$ nm, as determined from the data in Table 6 and the molecular-

Table 6. Weight-Average Molecular Weight M_w, z-Average Mean-Square Radius of Gyration $\langle s_i^2\rangle_z^{0.5}$, and Second Osmotic Virial Coefficient $\langle A_{ii}/M_i^2\rangle^{Ls}$ for the Systems Water (1) + PEG (2) and Water (1) + Dextran (3) at 293.15 K[a]

polymer	$M_{n,i}^{SEC}$	$M_{w,i}^{SEC}$	$M_{w,i}$	$\langle s_i^2\rangle_z^{0.5}$ (nm)	$10^3\langle A_{ii}/M_i^2\rangle^{Ls}$ [(cm³ mol)/g²]
PEG 1550	1 540	1 580	1 590		2.963
PEG 3000	2 840	2 880	2 880		2.611
dextran 40 000	21 200	37 600	36 960	9.7	0.616
dextran 70 000	56 800	67 700	67 940	14.7	0.421
dextran 110 000	64 800	109 400	113 070	22.7	0.352
dextran 500 000	110 000	418 000	530 610	70.7	0.302

[a] The molecular weights M_n and M_w of the polymers have also been determined by SEC.[13]

weight distributions of the dextrans.[13] These results indicate a high degree of flexibility of dextran in water.

References and Notes

(1) McMillan, W. G., Jr.; Mayer, J. E. *J. Chem. Phys.* **1945**, *13* (7), 276.
(2) Flory, P. J. *Principles of Polymer Chemistry*; Cornell University Press: Ithaca, NY, 1953.
(3) Elias, H. G.; Lys, H. *Makromol. Chem.* **1966**, *92*, 1.
(4) Hill, T. L. *J. Chem. Phys.* **1959**, *30* (1), 93.
(5) Edmond, E.; Ogston, A. G. *Biochem. J.* **1968**, *109*, 569.
(6) Vink, H. *Eur. Polym. J.* **1971**, *7*, 1411.
(7) Albertsson, P.-A. *Partition of Cell Particles and Macromolecules*, 3rd ed.; J. Wiley & Sons: New York, 1986.
(8) Kula, M.-R.; Kroner, K. H.; Hustedt, H. *Adv. Biochem. Eng.* **1982**, *24*, 73.
(9) Haynes, C. A.; Blanch, H. W.; Prausnitz, J. M. *Fluid Phase Equilibria* **1989**, *53*, 462.
(10) Shishov, A. K.; Krivobokov, V. V.; Chubarova, Ye. V.; Frenkel, S. Ya. *Polym. Sci. USSR (Engl. Transl.)* **1981**, *23*, 1330.
(11) Kang, C. H.; Sandler, S. I. *Macromolecules* **1988**, *21*, 3088.
(12) Gaube, J.; Pfennig, A.; Stumpf, M. *J. Chem. Eng. Data* **1993**, *38* (1), 163.
(13) Connemann, M.; Gaube, J.; Leffrang, U.; Müller, S.; Pfennig, A. *J. Chem. Eng. Data* **1991**, *36* (4), 446.
(14) Kurata, M. *Thermodynamics of Polymer Solutions*; MMI Press: London, 1982.
(15) Koningsveld, R. *Br. Polym. J.* **1975**, *7*, 435.
(16) Kehlen, H.; Rätzsch, M. T. *Z. Phys. Chem. Leipzig* **1983**, *264* (6), 1153.
(17) Cotterman, R. L.; Prausnitz, J. M. *Ind. Eng. Chem. Process Des. Dev.* **1985**, *24*, 434.
(18) Cotterman, R. L.; Bender, R.; Prausnitz, J. M. *Ind. Eng. Chem. Process Des. Dev.* **1985**, *24*, 194.
(19) Stroud, A. H.; Secrest, D. *Gaussian Quadrature Formulas*; Prentice Hall: Englewood Cliffs, NJ, 1966.
(20) Sotobayashi, H.; Überreiter, K. *Z. Elektrochem.* **1962**, *66*, 838.
(21) Yamakawa, H. *Modern Theory of Polymer Solutions*; Harper & Row: New York, 1971; pp 146–183 and 220.
(22) Münster, A.; Diener, H. *IUPAC International Symposium on Makromolecules*, Wiesbaden; Blackwell: Oxford, U.K., 1959; Section II, B5.
(23) Schulz, G. V.; Hellfritz, H. *Z. Elektrochem.* **1953**, *57*, 835.
(24) Kirste, R.; Schulz, G. V. *Z. Phys. Chem.* **1961**, *27*, 301.
(25) Bawn, E. H.; Freeman, R. F. J.; Kamaliddin, A. R. *Trans Faraday Soc.* **1952**, *46*, 862.
(26) Cantow, H. J.; Schulz, G. V. *Z. Phys. Chem.* **1954**, *2*, 117.
(27) Casassa, E. F. *Polymer* **1960**, *1*, 169.
(28) Florin, E.; Kjellander, R. *J. Chem. Soc., Faraday Trans. 1* **1981**, *77*, 2053.
(29) Topliss, R. Techniques to facilitate the Use of Equations of State for Complex Fluid-Phase Equilibria. Ph.D. Thesis, University of California, Berkeley, 1985.
(30) Prausnitz, J. M.; Lichtenthaler, R. N.; de Azevedo, E. G. *Molecular Thermodynamics of Fluid-Phase Equilibria*, 2nd ed.; Prentice Hall: Englewood Cliffs, NJ, 1986; p 539.
(31) Gaube, J.; Pfennig, A.; Stumpf, M. *Fluid Phase Equilib.* **1993**, *83*, 365.
(32) Schmidt, M. Personal communication, Max-Planck-Institut für Polymerforschung, Mainz, 1991.
(33) Zimm, B. H. *J. Chem. Phys.* **1948**, *16*, 1093.
(34) Albrecht, A. C. *J. Chem. Phys.* **1957**, *27*, 1002.
(35) Springer, J. *Einführung in die Theorie der Lichtstreuung verdünnter Lösungen grosser Moleküle*; Skriptum: Fritz-Haber-Institut der Max-Planck-Geselschaft, Berlin-Dahlem, 1970.

MA946394U